energies

MDPI

Article

Maximizing Liquid Fuel Production from Reformed Biogas by Kinetic Studies and Optimization of Fischer–Tropsch Reactions

Firas K. Al-Zuhairi [1], Zaidoon M. Shakor [1] and Ihsan Hamawand [2,*]

[1] Chemical Engineering Department, University of Technology-Iraq, Baghdad 10066, Iraq; 150009@uotechnology.edu.iq (F.K.A.-Z.); zaidoon.m.shakor@uotechnology.edu.iq (Z.M.S.)
[2] Wide Bay Water Process Operations, Fraser Coast Regional Council, Urangan, QLD 4655, Australia
* Correspondence: ihsan.hamawand@gmail.com

Abstract: In the current work, the operating conditions for the Fischer–Tropsch process were optimized using experimental testing, kinetic modelling, simulation, and optimization. The experiments were carried out using a Ce-Co/SiO_2 catalyst to examine how operating parameters affected the conversion of CO and product selectivity. A power-law kinetic model was used to represent the reaction rates in a mathematical model that was created to replicate the Fischer–Tropsch synthesis (FTS). It was decided to estimate the kinetic parameters using a genetic optimization technique. The developed model was validated for a range of operating conditions, including a temperature range of 200–240 °C, a pressure range of 5–25 bar, a H_2/CO ratio of 0.5–4, and a space velocity range of 1000–5000 mL/g_{cat}·h. The mean absolute relative error (MARE) between the experimental and predicted results was found to be 11.7%, indicating good agreement between the experimental data and the predicted results obtained by the mathematical model. Optimization was applied to maximize the production of liquid biofuels (C_{5+}). The maximum C_{5+} selectivity was 91.66, achieved at an operating temperature of 200 °C, reactor total pressure of 6.29 bar, space velocity of 1529.58 mL/gcat·h, and a H_2/CO feed ratio of 3.96. The practical implications of the present study are maximizing liquid biofuel production from biomass and municipal solid waste (MSW) as a renewable energy source to meet energy requirements, reducing greenhouse gas emissions, and waste management.

Keywords: biogas; liquid biofuel; Fischer-Tropsch synthesis; kinetic modelling

Citation: Al-Zuhairi, F.K.; Shakor, Z.M.; Hamawand, I. Maximizing Liquid Fuel Production from Reformed Biogas by Kinetic Studies and Optimization of Fischer–Tropsch Reactions. *Energies* **2023**, *16*, 7009. https://doi.org/10.3390/en16197009

Academic Editor: Attilio Converti

Received: 14 August 2023
Revised: 26 September 2023
Accepted: 28 September 2023
Published: 9 October 2023

1. Introduction

In recent years, increasing energy consumption has resulted from evolution in different transportation and industrial sectors, expansion in the human community, and a changing role for fossil fuels in the climate crisis. Therefore, the prospect of strict regulations on fossil fuel exploration has opened up opportunities for increasing the production of clean energy [1,2]. The Fischer–Tropsch reaction (FTR) system is considered an appealing method of producing liquid fuels and feedstock materials for petrochemicals from unconventional sources of petroleum, including coal, natural gas, and biomass. This process involves converting a syngas mixture of H_2 and CO over many types of catalysts [3]. The distribution of products in the Fischer–Tropsch reaction depends mainly on the reaction conditions, including operating temperature, total pressure, gas hourly space velocity, and H_2/CO ratio, as well as catalyst types and their physical characteristics [4].

Anaerobic digestion (AD) of municipal solid waste and biomass is an important technology that allows for the generation of extra value in the form of biogas. This process is part of circular economic creativity for power production [5–7]. Biogas is a stimulating carbon source due to its CO_2 content, which can be used to convert it into different ratios of syngas (a mixture of H_2 and CO) through dry reforming after upgrading and transformation [8].

The liquid fuels produced via FTR are clean fuels with low contents of nitrogen, aromatics, and sulfur compounds. To maximize the production of liquid fuel, it is necessary to

choose a suitable catalyst, optimize reaction conditions, and develop a mathematical model to describe the reaction kinetics to achieve higher reactant conversion while minimizing the production of light hydrocarbons (C_1–C_4) and carbon dioxide gas [9–11]. Cobalt catalysts have been considered the most active catalysts for the production of high molecular weight hydrocarbons (C_{5+}) and have high resistance to deactivation [12]. Moreover, the characteristics of catalysts can be improved by adding promoters to modify the porosity and texture of the support, which leads to beneficial mechanical properties and attrition resistance. Furthermore, this improves the dispersion and reducibility of metal species [13].

The main prerequisite factors in the design, optimization, and simulation of industrial processes are kinetic modeling and kinetic description [14]. The power law kinetic model for Fischer–Tropsch reactions has been proposed in many studies, including CO, H_2, H_2O, CO_2, CH_4, C_2H_4, C_2H_6, C_3H_8, n-C_4H_{10}, i-C_4H_{10}, and C_{5+} over different catalysts. Additionally, each reaction's activation energy is shown in (Table 1).

Table 1. Fischer–Tropsch reactions and activation energy.

Reactions	E_j (kJ/mol) [15]	E_j (kJ/mol) [16]	E_j (kJ/mol) [11]	E_j (kJ/mol) [17]	E_j (kJ/mol) [14]
$CO + 3H_2 \rightarrow CH_4 + H_2O$	83.4239	15.693	83.5	99.79	101.15
$2CO + 4H_2 \rightarrow C_2H_4 + 2H_2O$	65.018	20.384	65.0	72.51	78.79
$2CO + 5H_2 \rightarrow C_2H_6 + 2H_2O$	49.782	15.607	49.8	48.51	59.95
$3CO + 7H_2 \rightarrow C_3H_8 + 3H_2O$	34.8855	16.406	34.9	31.03	33.73
$4CO + 9H_2 \rightarrow n - C_4H_{10} + 4H_2O$	27.7289	86.934	27.7	27.59	23.04
$4CO + 9H_2 \rightarrow i - C_4H_{10} + 4H_2O$	25.7301	81.753	25.7	10.14	17.83
$6.5CO + 12.23H_2 \rightarrow C_{6.05}H_{12.36}(C_{5+}) + 6.05H_2O$	23.5643	73.878	23.6	12.44	21.25
$CO + H_2O \rightarrow CO_2 + H_2$	58.8263	55.329	58.8	10.00	50.24

For Fischer–Tropsch systems, many researchers have studied reaction kinetics and optimization of reaction conditions extensively. Using the power law rate equation or an expression based on certain mechanistic hypotheses, these investigations seek to define the reaction rate. Mosayebi and Haghtalab [18] developed a detailed kinetic model for Fischer–Tropsch synthesis over a Co Ru/γ-Al_2O_3 catalyst using a fixed-bed reactor at a range of reaction conditions. The Langmuir–Hinshelwood–Hougen–Watts (LHHW) method was used to derive elementary reactions for FTS. Kinetic expressions for the formation of n-paraffin and olefin were developed by combining alkyl and alkenyl mechanisms without considering the readsorption and secondary reactions of olefins. The Levenberg–Marquardt method and a genetic algorithm approach were used to optimize the kinetic model parameters. They showed that the computed values of activation energy have good agreement with values obtained by other studies.

Atashi et al. [19] proposed a kinetic model for the hydrogenation of CO over Fe/Ce catalyst using a fixed-bed microreactor at a range of reaction conditions. The proposed Langmuir–Hinshelwood kinetic mechanism tried about 16 kinetic expressions for the consumption of CO and the interchange among adsorbed molecules of H_2 and CO. They found that the CO conversion increased with an increase in temperature, pressure, and higher molecular hydrocarbon due to the temperature increase.

Moazami et al. [14] developed a sequence of collective Fischer–Tropsch (FT) and water–gas shift reaction mechanisms to investigate the kinetics of FT synthesis over a 37% Co/SiO_2 catalyst at twelve different operating conditions. They used different dual methodologies to improve the reaction network model for the FT synthesis. They found that the originally developed kinetic model, which was built on the combination alkyl/alkenyl mechanism, aimed at FT reactions (for the production of paraffin and α-olefins).

Hatami et al. [20] prepared and characterized a cobalt catalyst held on carbon nanotubes. The catalyst was tested at a wide range of operating conditions for liquid hydrocarbon products by the Fischer–Tropsch reaction in a fixed-bed reactor. Eleven kinetic expressions for CO consumption were developed based on several mechanisms. The nonlinear regression method using the Levenberg–Marquardt method was used to estimate kinetic parameters and to obtain the best optimization. They showed that the best models for suggested elementary reactions included the formation of surface species as rate-determining steps instead of syngas adsorption.

Haghtalab et al. [21] utilized a Langmuir–Hinshelwood–Hougen–Watson (LHHW) alkyl mechanism for kinetic modeling of FTS. A fixed-bed reactor (FBR) was used for the FTS reactions over a Co–Ru/CNTs catalyst with a nanostructure. The parameters of the kinetic model were estimated under different operating conditions such as pressure, temperature, gas hourly space velocity, and the H_2/CO ratio. They noticed that the outcomes of the experimental results are consistent with the developed kinetic model.

Pandey et al. [1] developed a kinetic model for the Fischer–Tropsch reaction to describe reactant consumption and product distribution using a 20Co-0.5Re/γ-Al_2O_3 catalyst. The model was optimized against an experimental database over a variety of operating conditions, with and without water present in the feed. They displayed an average absolute relative variation of almost 23.3%. In addition, the model successfully predicted the effects of water in the feed on the kinetics rate.

Although there have been many studies dealing with the kinetic modeling of the Fischer–Tropsch reaction, little information is presented in the literature focused on maximizing liquid biofuel products for the FT process. Accordingly, the main topic of the present study is to modify the kinetic model to describe FT accurately and then optimize the operating conditions of the process (i.e., pressure, temperature, H_2/CO feed ratio, and space velocity) to increase the selectivity of desired liquid biofuel products (C_{5+}).

2. Experimental Section

2.1. Catalyst Preparation

The Ce-Co/SiO_2 catalyst was prepared using the incipient wetness impregnation (IWI) method, which involves similar steps to those described by [22]. First, a suitable quantity of support (Silica Engineering, Maidstone, UK) was calcined under airflow at 500 °C for 4 h to achieve morphological stability during subsequent applications. Then, an aqueous solution was derived from a mixture of Co $(NO_3)_2 \cdot 6H_2O$ (97% Merck purity) and Ce $(NO_3)_3 \cdot 6H_2O$ (98.5% Merck purity), and the target loading of 1 wt. % Ce and 10 wt. % Co was achieved by adjusting the solution concentration. Impregnation was carried out at 80 °C for 4 h with continuous stirring until 10 wt. % Co and 1 wt. % Ce were loaded onto the SiO_2 support. The catalyst was then dried at 110 °C for 12 h and calcined at 600 °C for 6 h.

2.2. The Characterization Techniques

The BET surface area, pore radius, and pore volume of the prepared catalysts and support (SiO_2) were obtained by N_2 physisorption using a Micromeritics ASAP 2020 plus (USA), which is a high-performance adsorption analyzer. Before testing, the temperature was gradually raised to approximately 200 °C, at which point the samples were evacuated to 0.07 bar and held for ten hours. Afterward, the properties of the samples were recorded.

An analysis was performed on a sample of calcined catalyst using a TCD-equipped TP-5000 analytical machine (Tianjin Xianquan Co., Ltd., Tianjin City, China) to conduct temperature-programmed reduction (TPR). To eliminate any water, 0.1 g of each sample was first purged at 400 °C in an argon flow, and was then cooled to room temperature. The samples were then subjected to TPR testing, where the temperature was raised by 10 °C/min in steps from 25 °C to 900 °C while the argon flow rate was 30 mL/min. The catalysts and their precursors' morphology were examined using a Scanning Electron Microscope (SEM) equipped with a Silicon Drift Detector (SDD)—X-Max from Oxford Instruments Group (Oxford Instruments plc, Abingdon, UK).

2.3. FTS Reaction

A fixed-bed (F-B) reactor (ID: 10 mm, L: 900 mm) filled with two grams of catalyst (Figure 1a,b) was used to evaluate the catalyst for long-chain hydrocarbon production over a range of different parameters, including 200–240 °C, 5–25 bar, 1000–5000 mL/gcat·h, and a 0.5–4 H_2/CO feed ratio. In the first step, the catalyst was heated with a continuous stream of argon and then subjected to in situ reduction between 200 and 600 °C at a rate of 5 °C/min under a flow rate of 30 m/min for twelve hours using 5% H_2/Ar.

The system was then gradually cooled to ambient temperature. After reduction, argon gas was used to heat and pressurize the system to the desired reaction conditions. A Brooks 5850-mass flow controller was used to introduce the reformed biogas into the reactor at the desired space velocity and H_2/CO ratio. Every time the reaction conditions changed, the catalyst bed was thermally treated with argon at a flow rate of 41.6 mL/min for three hours at 400 °C to eliminate any carbon atoms that had accumulated there and may have reduced the catalyst activity. Two types of gas chromatography were used to analyze the FTR composition products: an online gas chromatograph (Shimadzu-2014, Shimadzu Corp. Ltd., Tokyo, Japan) equipped with FID and TCD for the analysis of the gas phase and an offline gas chromatograph (Varian CP 3800, SpectraLab Scientific Inc., Markham, ON, Canada) equipped with FID for the analysis of the liquid phase.

(**a**)

Figure 1. *Cont.*

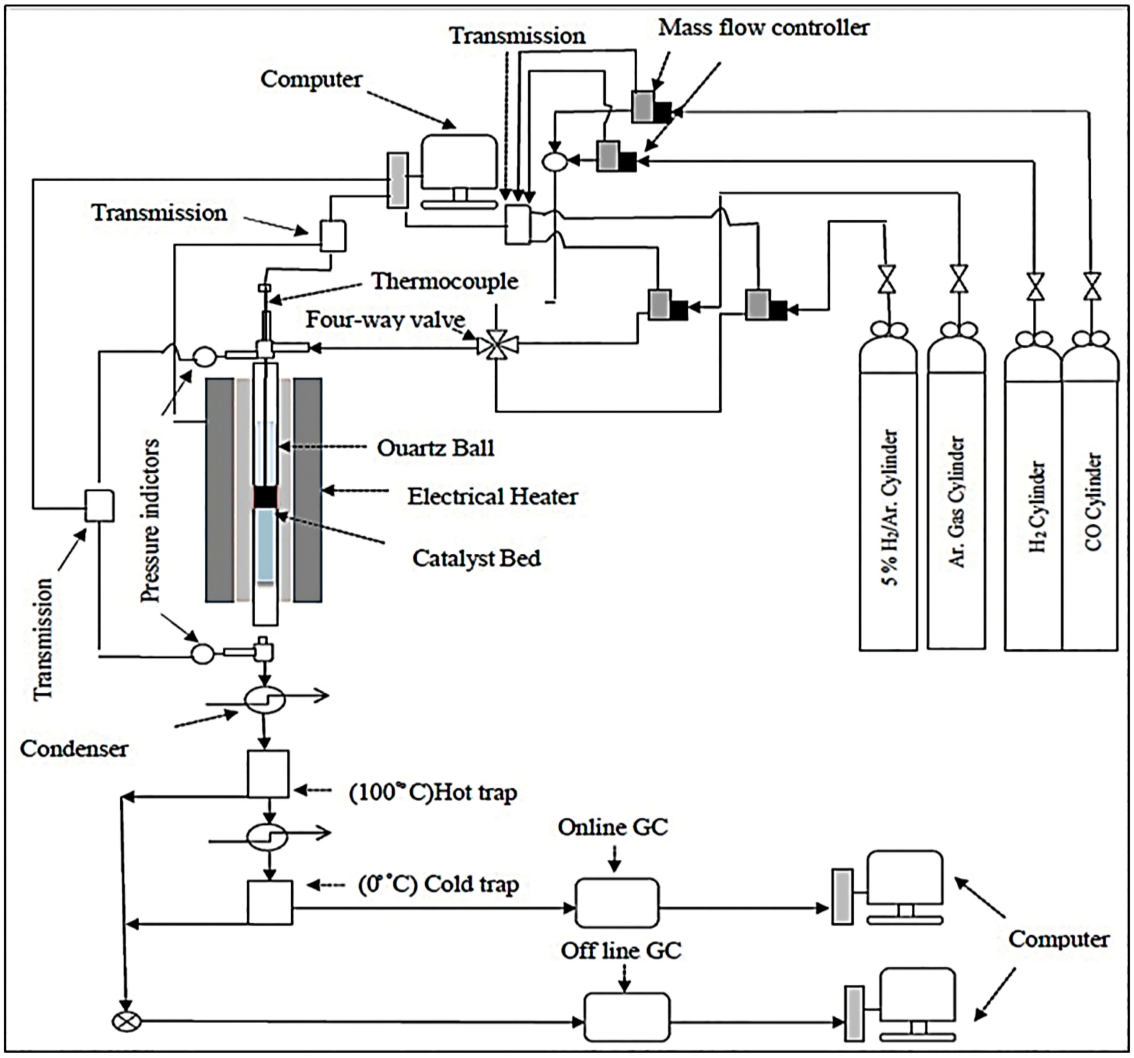

(**b**)

Figure 1. (**a**) View of the FTR experimental apparatus. (**b**) Schematic diagram of experimental setup.

The reactant conversions (i.e., CO) and product selectivity were calculated using Equations (1)–(4).

$$\text{CO Conversion } (\%) = \frac{\text{CO}_{\text{mole input}} - \text{ mole CO}_{\text{mole output}}}{\text{CO}_{\text{mole input}}} \times 100 \quad (1)$$

$$\text{Low} - \text{Chain Hydrocarbon Selectivity} = \text{S}_{\text{i }(\text{C}_1-\text{C}_4)}(\%) = \frac{\text{mole}_{\text{i}}}{\text{CO}_{\text{mole input}} - \text{ CO}_{\text{mole output}}} \times 100 \quad (2)$$

$$\text{Carbon Dioxide Selectivity } = \text{S}_{(\text{CO}_2)}(\%) = \frac{\text{Mole}_{\text{CO}_2}}{\text{CO}_{\text{mole input}} - \text{ CO}_{\text{mole output}}} \times 100 \quad (3)$$

$$\text{Total Liquid Selectivity } (\%) = \text{S}_{(\text{C}_{5+})}(\%) = 100 - \text{S}_{\text{i }(\text{C}_1-\text{C}_4)} - \text{ S}_{(\text{CO}_2)} \quad (4)$$

where:

$$\text{i} = CH_4,\ C_2\ H_4, C_2\ H_6, C_3\ H_6, n - C_4\ H_{10}, i - C_4\ H_{10}$$

3. Mathematical Modelling

3.1. Model Assumptions

The mathematical model was simplified using a number of simplification assumptions. The following are these presumptions:

- ❖ One-dimensional steady state model [14,23];
- ❖ Reactor's isothermal plug flow [24];
- ❖ Reactions in the homogeneous gas phase [25–27];
- ❖ Power law kinetic model [28,29].

3.2. Kinetic Model

The difference in the amounts of component *i* with respect to catalyst weight in the reactor bed is described by the following ordinary differential equation [30,31]:

$$\frac{dF_i}{dw} = -\sum_j^m s_{i,j} r_j \tag{5}$$

The power law reaction kinetic model shown in Table 1 was taken into consideration in this study, and the reaction rate was estimated using Equations (6) and (7):

$$r_j = k_j P_{CO}^{nj} P_{H2}^{mj} \text{ For reactions 1 to 7} \tag{6}$$

$$r_j = k_j P_{CO}^{nj} P_{H2O}^{mj} \text{ For reaction 8} \tag{7}$$

Eleven ordinary differential equations make up the reactor model, and Equation (5) was generalized for every component in the reaction mixture. The set of differential Equations (8)–(18) expresses the change in the molar flow rates with respect to catalyst weight within the fixed-bed reactor for CO, H_2, CH_4, C_2H_4, C_2H_6, C_3H_8, n-C_4H_{10}, i-C_4H_{10}, C_{5+}, CO_2, and H_2O, components, respectively [32].

$$\frac{dF_{CO}}{dW} = -r_1 - 2r_2 - 2r_3 - 3r_4 - 4r_5 - 4r_6 - 6.05r_7 - r_8 \tag{8}$$

$$\frac{dF_{H_2}}{dW} = -3r_1 - 4r_2 - 5r_3 - 7r_4 - 9r_5 - 9r_6 - 12.235r_7 + r_8 \tag{9}$$

$$\frac{dF_{CH_4}}{dW} = +r_1 \tag{10}$$

$$\frac{dF_{C_2H_4}}{dW} = +r_2 \tag{11}$$

$$\frac{dF_{C_2H_6}}{dW} = +r_3 \tag{12}$$

$$\frac{dF_{C_3H_8}}{dW} = +r_4 \tag{13}$$

$$\frac{dF_{i-C_4H_{10}}}{dW} = +r_5 \tag{14}$$

$$\frac{dF_{n-C_4H_{10}}}{dW} = +r_6 \tag{15}$$

$$\frac{dF_{C5+}}{dW} = +r_7 \tag{16}$$

$$\frac{dF_{CO_2}}{dW} = r_8 \tag{17}$$

$$\frac{dF_{H_2O}}{dW} = +r_1 + 2r_2 + 2r_3 + 3r_4 + 4r_5 + 4r_6 + 6.05r_7 - r_8 \tag{18}$$

The partial pressure of the *i*th component can be calculated according to Dalton's law:

$$P_i = y_i \times P_t = \frac{F_i}{\sum_i^N F_i} \times P_t \tag{19}$$

The fluctuation of the reaction rate constants with temperature was represented using the Arrhenius equation (Equation (20)).

$$k_j = k_j^o exp\left(-\frac{E_{Aj}}{RT}\right) \tag{20}$$

3.3. Assessment of Kinetic Parameters

To reduce the objective function (f) in Equation (21), which measures the mean relative deviation between the experimental and projected gas compositions of the reactor effluent, the kinetic parameters were calculated using an integration-optimization technique [33–35].

$$f = \frac{1}{n_{exp}} \sum_{i=1}^{n_{exp}} \left(\frac{1}{n_{Com}} \sum_{j=1}^{n_{Com}} \left| \frac{y_{i,j}^{exp} - y_{i,j}^{pred}}{y_{i,j}^{exp}} \right| \right) \times 100 \tag{21}$$

The eleven ordinary differential equations were numerically integrated using the 4th. The Runge–Kutta integration method for each set of kinetic parameters, and a global optimal set of kinetic parameters was estimated using a genetic algorithm. The "*ga*" and "*ode45*" Matlab subroutines were used for optimization and integration, respectively. The major steps of the genetic algorithm are depicted in a flowchart in (Figure 2).

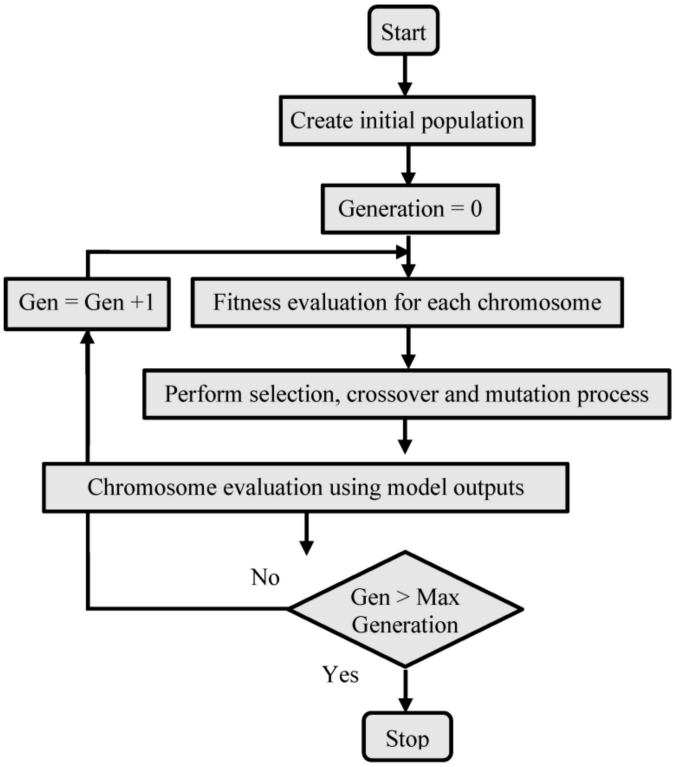

Figure 2. Flowchart of computational procedure of genetic algorithm.

4. Results and Discussion

This part is presented in two sections. In the first Section 4.1, the results of the experimental studies are presented, while in Section 4.2, the focus is on the results of the parametric optimization and kinetic studies for converting reformed biogas to liquid fuel.

4.1. Results of Experimental Studies

4.1.1. Catalyst Characterization

The textural characteristics of the prepared catalysts and support, which include surface area, pore radius, and pore volume, are presented in Table 2. It can be observed that the loading of metals (Ce and Co) on the support (SiO_2) reduces the surface area by around 9.2% and 11.5% for $10Co/SiO_2$ and $1Ce\text{-}10Co/SiO_2$, respectively. The reduction in surface area of the support, due to metals partially blocking its pores, implies that the metals were effectively incorporated into its porous structure [36,37].

Table 2. Textural characteristics of support and catalysts.

Sample	BET SA (m^2/g)	Pore Volume (cm^3/g)	Pore Radius (nm)
SiO_2	226	0.51	9
$10Co/SiO_2$	205	0.43	8.6
$1\ Ce^{-}10Co/SiO_2$	200	0.42	8.4

In order to predict the reducibility behavior of the prepared catalysts, H_2-TPR analysis was performed for the $10Co/SiO_2$ and $1Ce\text{-}10Co/SiO_2$ catalysts under the same conditions as shown in (Figure 3). The results showed a pair of reduction peaks for the $10Co/SiO_2$ catalyst at temperatures of 335 °C and 535 °C, corresponding to the reduction of Co_3O_4 to CoO and CoO to Co metal, respectively. Moreover, the addition of Ce metal as a promoter reduced the reduction peaks by about 25 °C and 18 °C, respectively. These results demonstrate that Ce metal can reduce Co^{3+} to Co^{2+} ions at a lower temperature than the cobalt oxides in the $10Co/SiO_2$ catalyst [38]. Similar patterns of behavior were observed by [39,40].

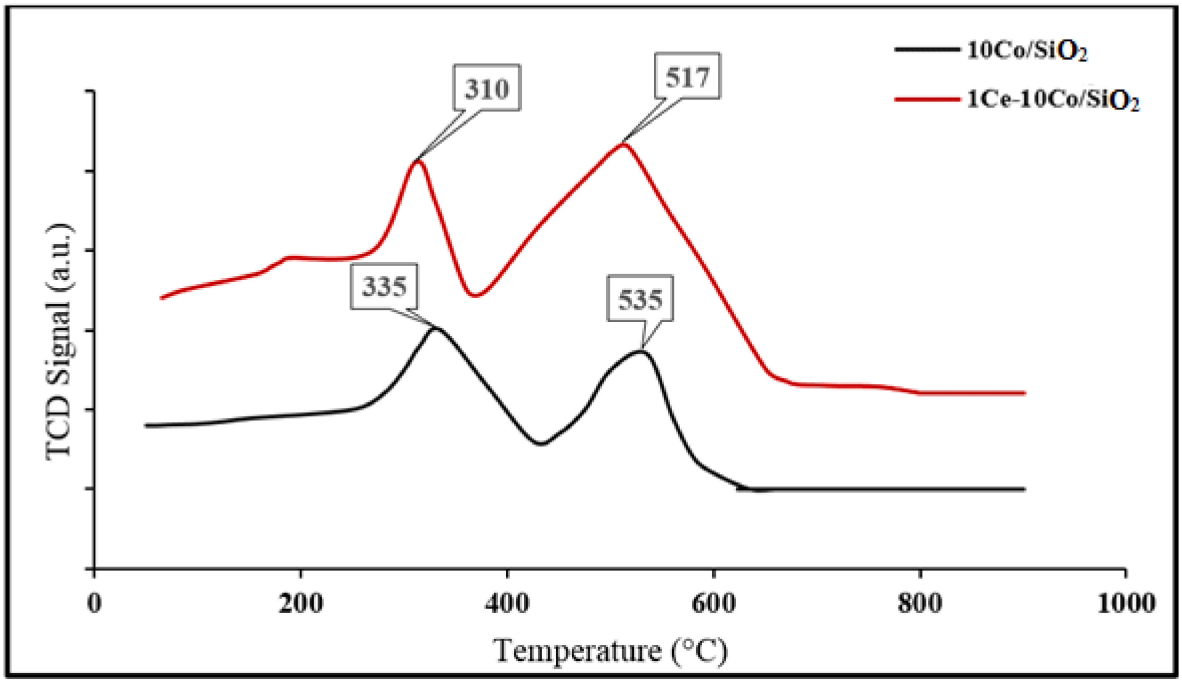

Figure 3. H_2-TPR patterns for cobalt-based catalysts.

Accordingly, the H_2-TPR results show that the chosen conditions (5 vol. % H_2, flow rate of 30 m/min, and a duration of 12 h) are suitable for reducing Co_3O_4 to Co metal prior to the beginning of FTR.

A comprehensive scanning electron microscope (SEM) study was conducted to examine the morphological changes of the catalysts and their precursors at different stages: before and after the test. The SEM images captured during the analysis are presented in Figure 4. Notably, distinct differences were observed in the morphology of the catalyst precursor (Figure 4a) and the calcined catalyst (Figure 4b). The electron micrograph of the catalyst precursor displayed numerous agglomerates of particles, indicating a less dense structure. However, after calcination at 600 °C, the morphology significantly transformed, with reduced agglomeration evident in the calcined catalyst (Figure 4b). This transformation was attributed to the coverage of the calcined catalyst surface with small crystallites of cobalt and cerium oxide [41]. Moreover, following the Fischer–Tropsch synthesis (FTS) chemical reaction, the catalyst underwent further changes in texture and morphology (Figure 4c). Notably, the grain size of the tested catalyst increased, primarily due to agglomeration resulting from sintering after the reactions. These SEM observations provided valuable insights into the structural modifications and behavior of the catalysts during the various stages of the study.

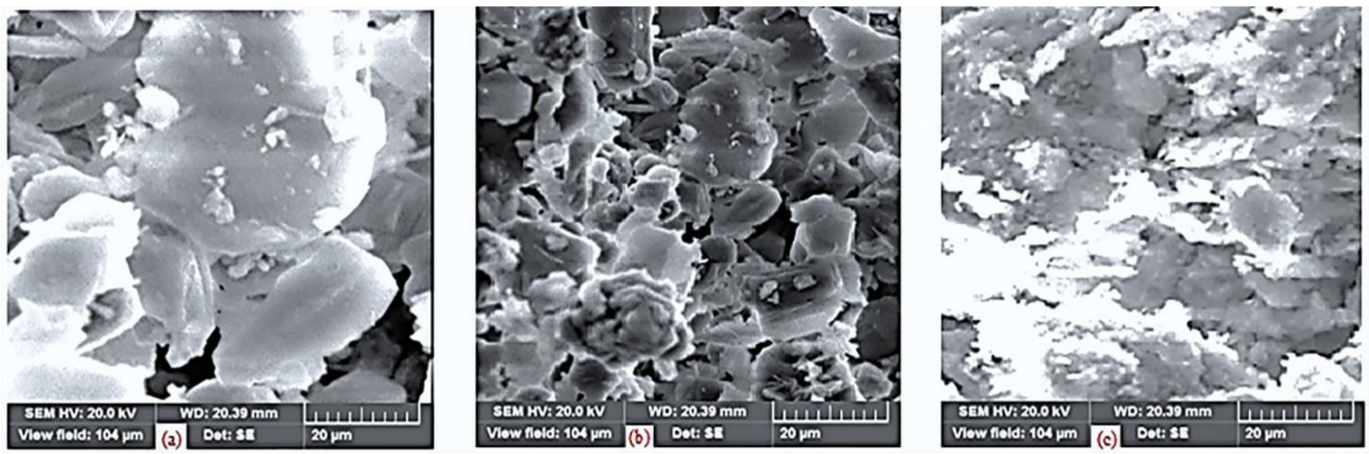

Figure 4. SEM images of the catalyst: (**a**) precursor, (**b**) before the test, and (**c**) after the test.

4.1.2. Effects of Variables on FTS

The effects of different reaction conditions, such as operating temperature (200–240 °C), total pressure (5–25 bar), space velocity (1000–5000 mL/gcat·h), and H_2/CO (0.5–4) on the experimental results for CO conversion and product selectivity are presented in (Figures 5–8) and summarized in (Table 3).

As shown in (Figure 5), the CO conversion and low-chain hydrocarbons selectivity (CH_4, C_2–C_4) and CO_2 increased with increases in reaction temperature from 200 to 240 °C. In contrast, the selectivity of total liquid biofuel products (C_{5+}) decreased by about 21.4%. The decrease in total liquid products is attributed to the fact that the Fischer–Tropsch reaction is an exothermic polymerization reaction. Furthermore, at higher reaction temperatures, the rate of hydrogenation of "CH_2" units accelerated, shifting the product selectivity towards lower-chain hydrocarbons [42,43]. Given these important findings, a lower reaction temperature of 200 °C is recommended for obtaining the best selectivity of liquid biofuel products (C_{5+}).

Based on thermodynamic principles, increasing the total pressure of the reaction unit shifts the equilibrium reactions towards the products, leading to an increase in reactant conversion. Therefore, the effect of total pressure on the activity of the catalyst and the product selectivity was investigated and presented in Figure 6. The results indicate that the conversion of CO and the formation of desired products (C_{5+}) increased by about

58.9% and 2.1%, respectively, when the total pressure was increased from 5 to 25 bar. On the other hand, the selectivity of lower chain hydrocarbons and CO_2 decreased, which is consistent with an increase in chain growth probability with increasing pressure [44]. Using the outcomes of these trials, it can be said that high pressure (25 bar) is the optimal choice for producing liquid biofuel products (C_{5+}) in the range of reaction pressures tested (5–25 bar), with a reaction temperature of 200 °C, a space velocity of 1000 mL/gcat·h, and an inlet feed ratio of 0.5 (H_2/CO).

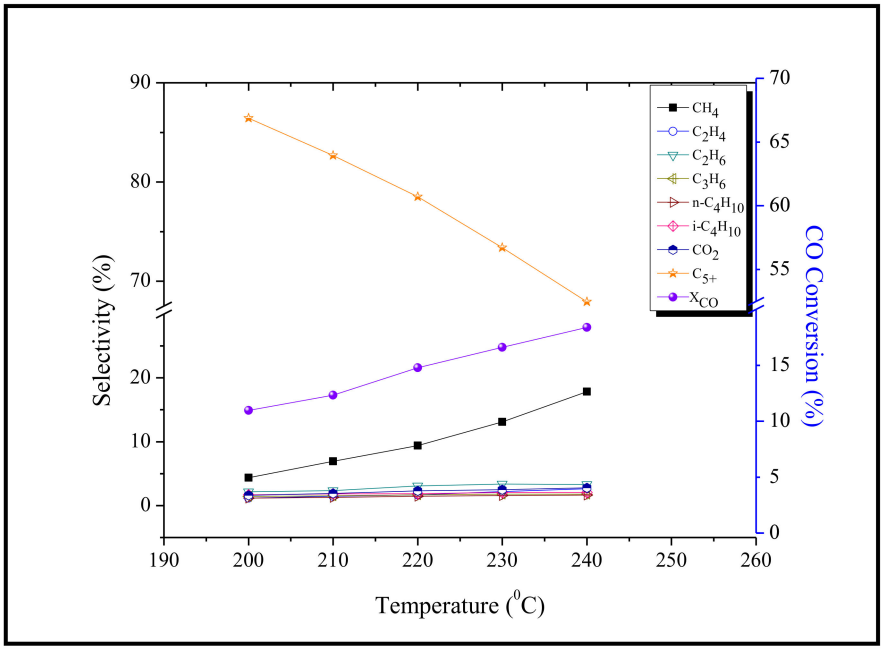

Figure 5. Effects of temperatures on the CO conversion and products selectivity at 5 bar, 1000 mL/gcat·h, and H_2/CO = 0.5.

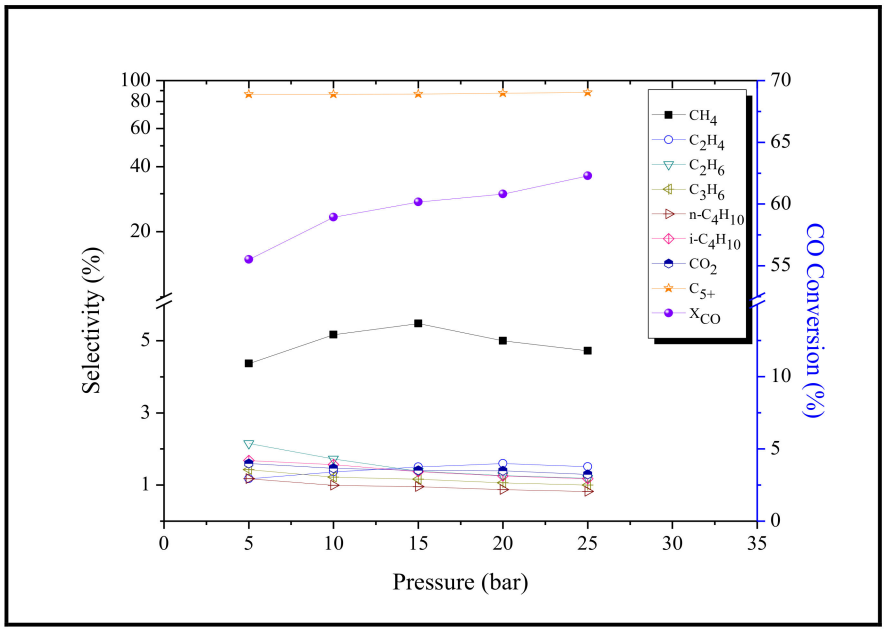

Figure 6. Effects of total pressure on the conversion of CO and products selectivity at 200 °C, 1000 mL/gcat·h, and H_2/CO = 0.5.

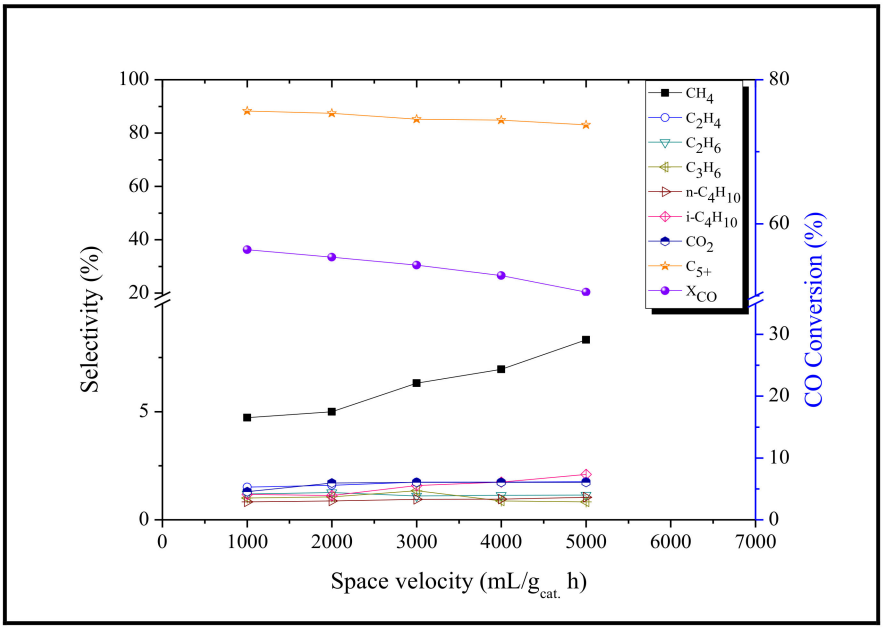

Figure 7. Effect of space velocity on the conversion of CO and products selectivity at 200 °C, 25 bar, and $H_2/CO = 0.5$.

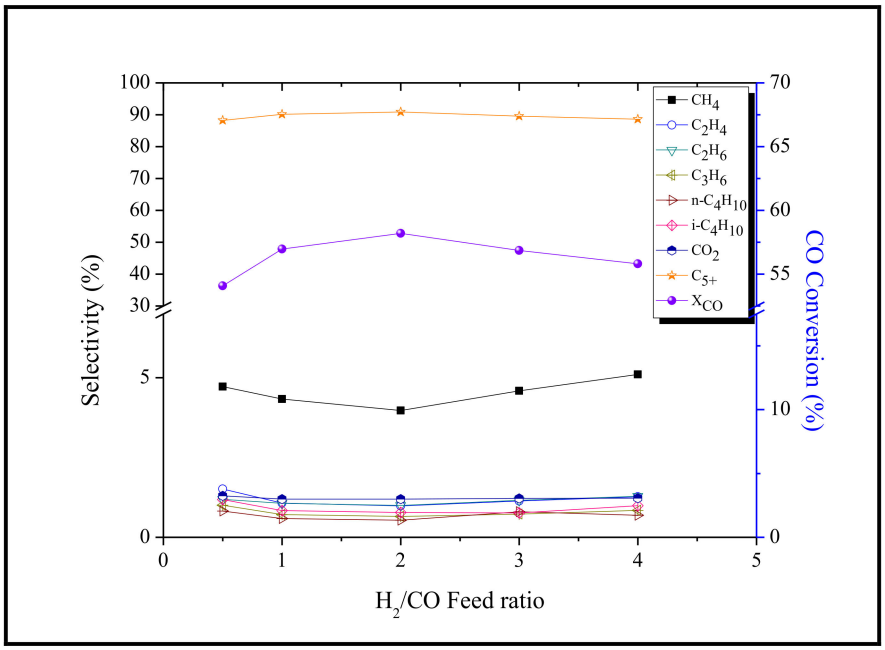

Figure 8. Effect of proportion of inlet feed (H_2/CO) on the conversion of CO and products selectivity at 200 °C, 25 bar, and 1000 mL/$g_{cat.}$ h.

To understand the effect of residence time on reactant conversion and product selectivity, a series of experiments were conducted at different space velocities, as shown in (Figure 7). It can be observed that increasing the space velocity from 1000 to 5000 mL/gcat·h, resulted in decreases in the formation of desired hydrocarbons (C_{5+}) and the conversion of CO by around 6% and 43.8%, respectively. Conversely, the formation of lower chain hydrocarbons (CH_4 and C_2–C_4) increased. The low production of CO_2 is in agreement with the lower WGS activity typically observed with cobalt catalysts [45]. Increasing the space velocity reduces the residence time of the reaction, which in turn reduces chain growth and reactant conversion, leading to a hasty increase in the production of low-chain hydrocarbons and a decrease in the production of total liquid products (C_{5+}) [46]. Accord-

ing to the experimental results, a lower space velocity of 1000 mL/gcat·h is the optimal choice for producing favorable liquid biofuel (C_{5+}) in the range of space velocities tested (1000–5000 mL/gcat·h), with a reaction temperature of 200 °C, a total pressure of 25 bar, and an inlet feed ratio of 0.5 (H_2/CO).

Table 3. Experimental results at different operation conditions using the 1Ce-10Co/SiO_2 catalyst.

T (°C)	P (bar)	Sv (mL/gcat·h)	H_2/CO	$\%X_{CO}$	Experimental Products Selectivity (%)							
					CH_4	C_2H_4	C_2H_6	C_3H_6	n-C_4H_{10}	i-C_4H_{10}	CO_2	C_{5+}
200	5	1000	0.5	14.9	4.368	1.176	2.150	1.428	1.176	1.680	1.600	86.422
210	5	1000	0.5	17.3	6.954	1.464	2.342	1.556	1.281	1.830	1.900	82.673
220	5	1000	0.5	21.6	9.405	1.672	3.093	1.672	1.463	1.881	2.300	78.514
230	5	1000	0.5	24.8	13.108	2.192	3.390	1.808	1.582	2.034	2.500	73.386
240	5	1000	0.5	27.9	17.850	2.627	3.290	1.785	1.658	2.066	2.800	67.926
200	5	1000	0.5	14.9	4.368	1.176	2.150	1.428	1.176	1.680	1.600	86.422
200	10	1000	0.5	23.4	5.170	1.368	1.728	1.224	0.994	1.570	1.468	86.479
200	15	1000	0.5	27.5	5.480	1.507	1.384	1.165	0.959	1.370	1.410	86.726
200	20	1000	0.5	29.9	5.000	1.600	1.263	1.063	0.875	1.250	1.400	87.550
200	25	1000	0.5	36.3	4.720	1.510	1.192	1.003	0.826	1.180	1.300	88.269
200	25	1000	0.5	36.3	4.720	1.510	1.192	1.003	0.826	1.180	1.300	88.269
200	25	2000	0.5	33.5	5.000	1.600	1.263	1.063	0.875	1.125	1.700	87.375
200	25	3000	0.5	30.5	6.320	1.738	1.106	1.343	0.948	1.580	1.730	85.235
200	25	4000	0.5	26.6	6.960	1.740	1.131	0.870	0.957	1.740	1.735	84.867
200	25	5000	0.5	20.4	8.320	1.768	1.144	0.832	1.040	2.101	1.734	83.061
200	25	1000	0.5	36.3	4.720	1.510	1.192	1.003	0.826	1.180	1.300	88.269
200	25	1000	1	47.9	4.334	1.075	1.067	0.714	0.588	0.840	1.200	90.182
200	25	1000	2	52.8	3.973	0.986	1.001	0.655	0.539	0.778	1.200	90.869
200	25	1000	3	47.4	4.592	1.139	1.157	0.730	0.801	0.765	1.220	89.595
200	25	1000	4	43.2	5.108	1.267	1.287	0.842	0.693	0.990	1.230	88.583

Figure 8 presents the effect of different inlet feed ratios on catalyst activity and product selectivity at 200 °C, 25 bar, and 1000 mL/gcat·h The results show that increasing the proportion of inlet feed from 0.5 to 2 reduces the formation of low-chain hydrocarbons and increases selectivity for the desired product (C_{5+}) and CO conversion by about 3% and 31.3%, respectively. However, increasing the proportion of inlet feed from two to four results in a decrease in reactant conversion and desired product selectivity (C_{5+}) of about 18.2% and 2.5%, respectively. The change in reactant concentration within the proportion of inlet feed has a considerable effect on its partial pressure. At a proportion of feed less than two, the H_2 partial pressure will decrease, causing some CO molecules to escape without being hydrogenated. At a proportion greater than two, the H_2 partial pressure will increase, leading to a decrease in catalyst activity [47,48]. Therefore, the best option for producing the desired products is an inlet feed ratio of two.

4.2. Results of Parametric Optimization and Kinetic Studies

4.2.1. Model Validation

The procedure for estimating kinetic parameters depends on minimizing the mean absolute relative error (MARE) obtained between the experimental and predicted results. The genetic optimization method initially generates a number of chromosomes, with each chromosome representing a different set of kinetic parameters. Each chromosome is evaluated by applying its kinetic parameters in a mathematical model to simulate the response corresponding to sixteen experiments and predict the MARE for each one of these chromosomes. The optimization process continues until the MARE reaches its minimal

value, and this chromosome represents the optimum kinetic parameters. The parity plot for the comparison of the experimental data from 16 experiments with the expected findings for CO, CH_4, C_2H_4, C_2H_6, C_3H_8, n-C_4H_{10}, i-C_4H_{10}, C_{5+}, and CO_2 is shown in Figure 9. The simulation results at the optimum kinetic parameters are also shown in Table 4. Bench assesses the accuracy of the fitted model by utilizing a quantitative analysis approach and the MARE (11.7%) to compare the acquired results by the fitted model with those estimated by experiments (Table 3), with respect to CO conversion and product selectivity. The good accuracy of the fitted model is in comparison with the values reported by [1] (23.1%); [49] (20%); and [50] (48.4%). The minimum error is recognized for C_{5+} (MARE = 2.5%), while the maximum error obtained is for remaining CO (MARE = 27.7%). These confirm that the modified model accurately estimates the production rate of liquid biofuels (C_{5+}). The MARE for CO is relatively higher than that for other components because the conversion of CO is high, and the remaining quantities of CO in the reactor effluent are too low. Therefore, higher levels of relative errors occur when comparing the experimental CO concentrations with the predicted CO concentrations in the reactor effluent. The modeling results agree very well with the experimental data, especially in predicting C_{5+} selectivity.

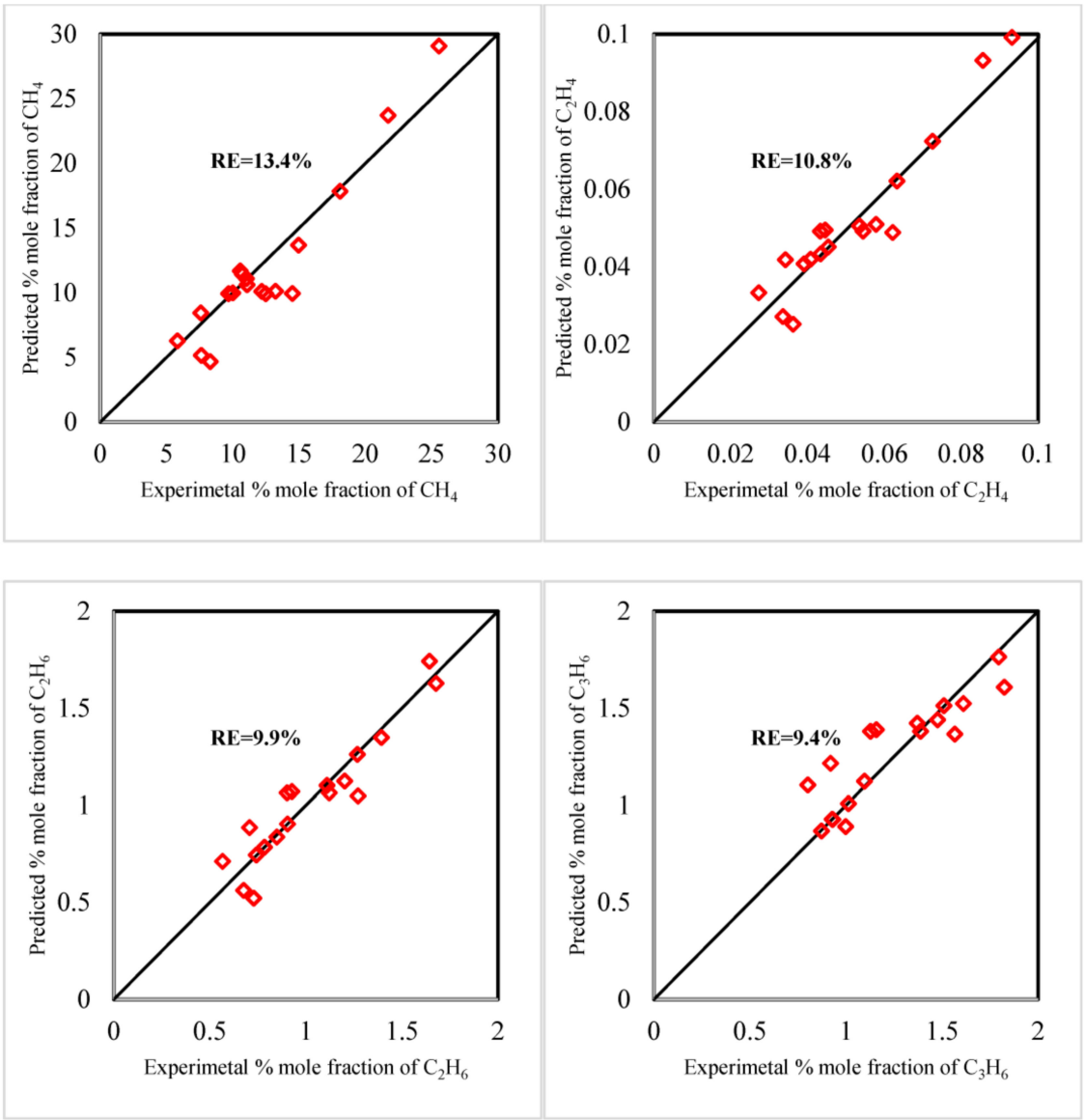

Figure 9. *Cont.*

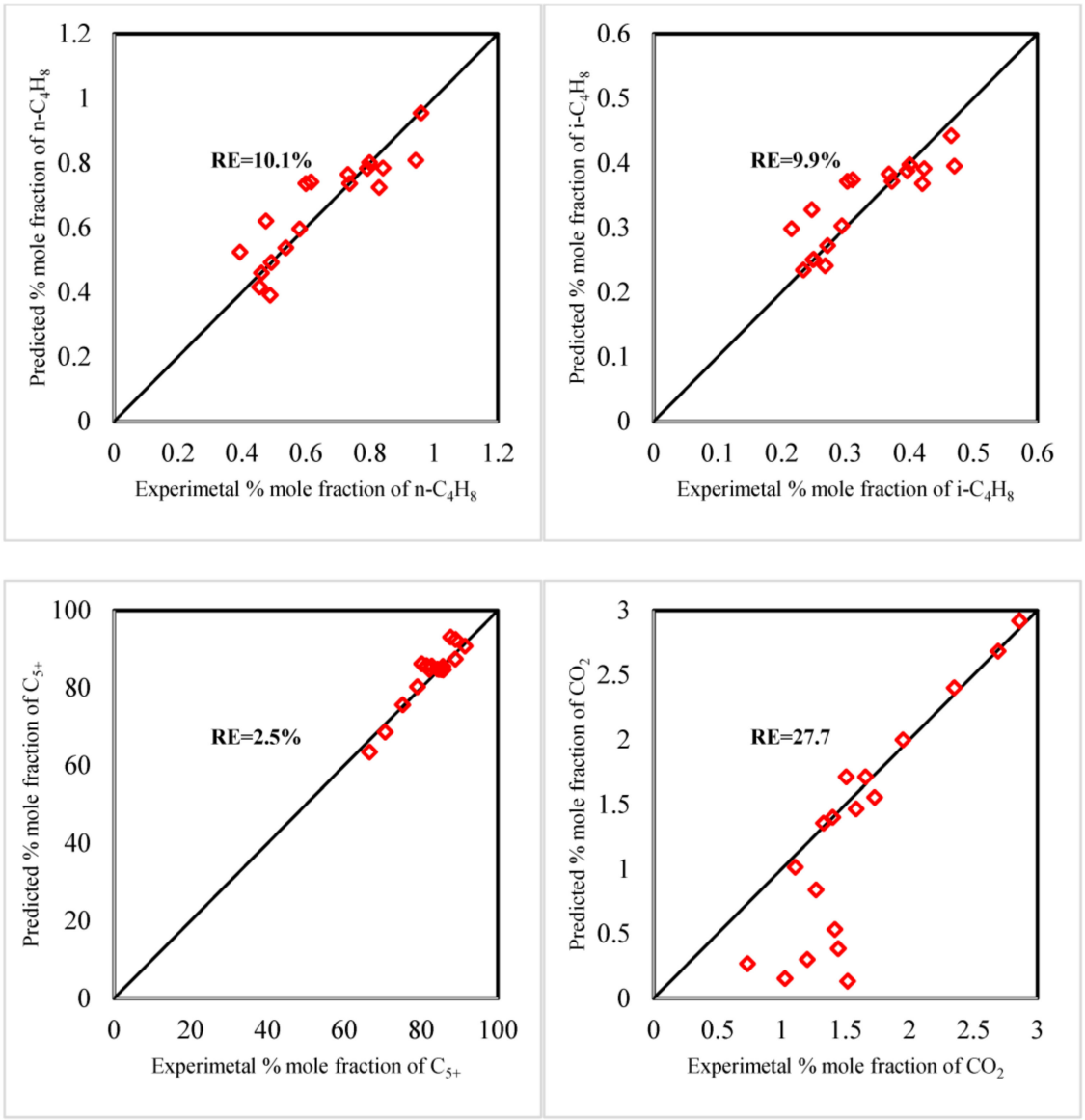

Figure 9. Parity plot comparing experimental data and results predicted by a power-law rate model for CO_2, CO, CH_4, C_2H_4, C_2H_6, C_3H_8, n-C_4H_{10}, and i-C_4H_{10}.

The optimized values of the kinetic model parameters are given in (Table 5). A higher activation energy (80.214 kJ/mol.) was found for methane formation, while a lower activation energy was found for C_{5+} formation. By comparing the activation energies obtained from this study with those obtained from previous studies, it can be observed that a similar range of activation energies (12.86–80.21 kJ/mol.) was obtained in the present study compared with that obtained in previous kinetic works [14–16], which was in the range of 10–101.15 kJ/mol. The estimated activation energies for C_{5+} formation (12.86) are also within those reported in the literature [14,15,17], which are in the range of 12.44–23.56. The estimated values of the kinetic parameters are shown in Table 5.

Table 4. Predicted results at different operation conditions using the 1Ce-10Co/SiO_2 catalyst.

T (°C)	P (bar)	Sv (mL/gcat·h)	H_2/CO	$\%X_{CO}$	Predicted Products Selectivity (%)							
					CH_4	C_2H_4	C_2H_6	C_3H_6	n-C_4H_{10}	i-C_4H_{10}	CO_2	C_{5+}
200	5	1000	0.5	15.3	4.271	1.176	2.153	1.430	1.180	1.766	1.674	86.351
210	5	1000	0.5	18.1	6.434	1.462	2.318	1.547	1.281	1.811	1.900	83.247
220	5	1000	0.5	21.0	9.406	1.784	2.474	1.662	1.377	1.854	2.153	79.289
230	5	1000	0.5	23.8	13.309	2.130	2.620	1.777	1.468	1.901	2.454	74.340
240	5	1000	0.5	25.4	18.173	2.475	2.733	1.881	1.541	1.950	2.888	68.359
200	5	1000	0.5	15.3	4.271	1.176	2.153	1.430	1.180	1.766	1.674	86.351
200	10	1000	0.5	25.0	4.571	1.398	1.744	1.296	1.058	1.583	1.344	87.005
200	15	1000	0.5	25.1	4.750	1.507	1.461	1.146	0.941	1.374	1.421	87.399
200	20	1000	0.5	25.5	4.878	1.596	1.305	1.067	0.876	1.270	1.400	87.608
200	25	1000	0.5	25.7	4.980	1.667	1.192	1.003	0.827	1.180	1.367	87.785
200	25	2000	0.5	24.7	5.031	1.660	1.147	0.946	0.797	1.077	0.602	88.740
200	25	3000	0.5	24.2	5.049	1.655	1.130	0.926	0.785	1.044	0.343	89.069
200	25	4000	0.5	20.5	5.063	1.620	1.069	0.861	0.744	0.949	0.256	89.437
200	25	5000	0.5	17.2	5.069	1.602	1.043	0.833	0.725	0.910	0.212	89.606
200	25	1000	0.5	25.7	4.980	1.667	1.192	1.003	0.827	1.180	1.367	87.785
200	25	1000	1	49.7	4.884	1.458	1.143	0.870	0.756	0.969	1.039	88.882
200	25	1000	2	54.9	4.709	1.198	1.109	0.741	0.684	0.782	0.866	89.911
200	25	1000	3	47.6	4.592	1.092	1.157	0.730	0.684	0.765	0.928	90.051

Table 5. The optimal values of the kinetic parameters for the current kinetic model.

Reaction No.	A_o (mol/$gm_{cat.}$h)	E (kJ/mol)	n_j	m_j
1	148.889688	80.214	0.82	0.60
2	0.005413	60.424	0.25	0.08
3	0.002886	45.814	0.69	0.55
4	0.000147	32.495	0.16	0.13
5	0.000029	28.932	0.66	0.54
6	0.000012	27.871	0.09	0.42
7	0.000071	12.861	0.55	0.63
8	0.000125	37.850	0.13	0.22

4.2.2. Process Optimization

The goal of the optimization study was to increase the selectivity of liquid biofuel, in particular the selectivity of higher-molecular-weight hydrocarbons like C_{5+}, as well as to increase synthesis gas conversions (particularly CO conversion) and decrease the forming of unwanted products like carbon dioxide and methane. For each of these variables, Table 6 includes a set of randomly chosen values together with the best result from the optimization process. In particular, C_{5+} hydrocarbon productivity was increased by the optimization of the working conditions. In light of this, the objective function equation is as follows:

$$\text{Obj} = \text{maximize}(S_{C5+/\text{Undesired}}) = \frac{F_{C5+}}{F_{Co2} + F_{CH4} + F_{C2H4} + F_{C2H6} + F_{C3H6} + F_{n-C4H8} + F_{i-C4H8}} \quad (22)$$

Table 6. Genetic optimization table.

Iteration No.	Temperature (°C)	Pressure (bar)	GHSV (mL/g_{cat}·h)	H_2/CO	C_{5+} Selectivity
1	203.62	9.96	2431.98	2.55	48.144
2	203.62	22.41	4679.28	1.08	48.144
3	239.85	22.41	4679.28	2.83	48.144
4	203.62	22.41	4679.28	1.08	48.144
5	239.17	17.00	2720.28	1.82	56.916
9	203.62	16.83	4648.61	1.82	57.596
13	201.92	22.31	4648.61	1.52	60.792
16	227.56	17.61	3854.65	2.89	61.268
18	201.92	13.98	1626.90	2.55	77.112
20	204.16	22.41	1914.13	3.89	80.784
28	211.32	6.59	1914.13	3.41	81.396
41	206.51	6.59	1798.41	3.41	81.464
57	202.50	18.79	4808.26	3.70	82.28
59	202.50	22.82	1171.16	3.70	82.348
94	201.00	13.84	1023.51	3.84	88.264
100	202.91	15.11	3885.25	3.85	88.672
120	216.15	5.20	1023.51	3.85	89.284
124	237.44	6.10	1067.01	3.66	89.556
240	200.65	6.21	1638.91	3.81	89.692
286	200.11	15.96	1012.16	2.78	91.12
446	200.11	6.21	3206.02	3.06	91.188
851	200.09	6.21	1513.96	3.90	91.188
852	230.41	6.21	1513.96	3.70	91.46
1000	200.09	6.29	1529.58	3.96	91.664

Table 6 lists the outcomes of genetic optimization, and (Figure 10) shows how the objective function changes as the number of iterations increases (generation number). After the highest possible generation count (1000) is achieved, the optimizer ends. At these operating conditions: 200 °C temperature, 6.29 bar reactor total pressure, 1529.58 mL/gcat·h space velocity, and a H_2/CO feed ratio of 3.96, the maximum C_{5+} selectivity was achieved at 91.66.

We should monitor here that liquid biofuel generated by integration of the Fisher–Tropsch process with anaerobic digestion reduces greenhouse gas emissions in comparison with conventional fossil fuels and contributes to meeting renewable transportation fuel standards [51]. Additionally, capital, operating costs, and the lower trade price of the system are directly proportional to the feed capacity of the plant; if the feed capacity is increased, the selling price is decreased. The lowermost trade price of FT liquid fuels derived from biogas for a plant capacity of 2000 m^3/h was around \$5.29/GGE, but at a larger plant size, the trade price was \$2.37/GGE and \$1.92/GGE for plant capacities of 10,000 and 20,000 m^3/h, respectively. In other words, the economy of this technology is based mainly on operating costs, biogas costs, and the conversion rate of FTS [52]. Through investigating high- and low-temperature operating modes, [8], revealed that tri-reforming for the invention of FT liquid fuels from biogas, taking into account the biogas as rubbish with zero cost and from a plant supplied with waste, enhanced syngas production. The cost of the generation for a plant that receives 12 Mm^3 of biogas/year is \$3/gallon for

HTFT and $1.7/gallon for LTFT. Naqi et al. [53], reported the liquid fuel derived from integration of the AD and FTR requires a capital expenditure of around $210/ton of biomass and operational expenses of around $110/ton of biomass for a plant capacity of 90,000 tons/year. In another, a number of studies were carried out by [54–56] to evaluate the techno-economic assessment for converting various kinds of biomass to liquid fuel, they established that the product cost alternated from $2.86 to $4.61 per GGE.

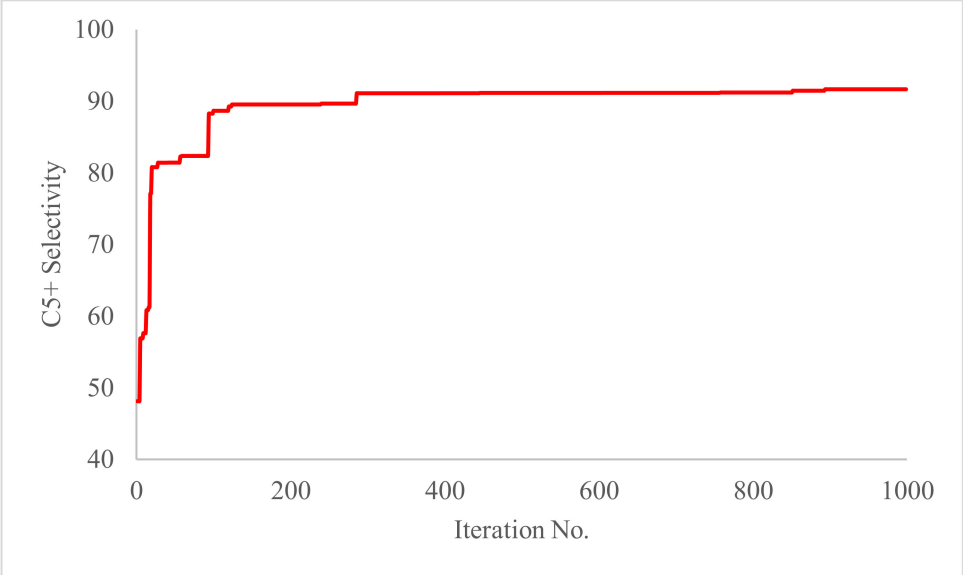

Figure 10. Objective function changes as the number of iterations.

In order to evaluate the environmental effect of liquid fuel generated from biogas using FTS, [51] accomplished a life cycle analysis to create liquid fuel (diesel) from biogas. Crop cultivation as feedstocks for the anaerobic digestion system, harvest, and transport to the bio-refinery, biomass to Fischer–Tropsch liquid (BTL), and combustion of liquid fuel for a passenger car were all considered in the analysis. By comparison with classic fossil-derived diesel, they confirmed how biogas-derived liquid fuel might decrease greenhouse gas emissions by about 73%. Generally, in comparison to liquid fuel conversion practices from biomass to their traditional fossil fuel equivalent, they display lesser climate variation capacity and GHG emissions. The normal reduction in GHG emissions from biofuels prepared from first-generation feedstock is between 50 and 75% [57,58]. However, compared with first-generation biofuels, second-generation biofuels have a higher possibility of cutting GHG emissions by 50–100% [59]. GHG emissions may be decreased by approximately 76% using third-generation feedstock [60].

The work of the dynamic metals employed in FT catalysts, and the comparison of anticipated lifetimes, is another critical highlight of FTS. Practically, 25–30% of the CO consumed in FTR was used by press catalysts, which are motivated by the generation of CO_2 through the water–gas shift reaction. Also, the water vapor delivered amid the union prevents CO from being changed over to hydrocarbons, which brings down the reaction rate within the press catalyst's lower layers [61]. These problems are not shown with cobalt catalysts. Water has a small impact on the reaction, and the selectivity of CO_2 generation on it often does not surpass a number of percent [62,63]. Moreover, the presence of water vapor makes steps in the selectivity of cobalt catalysts for the desired higher hydrocarbons simpler; advancement of Cobalt catalysts with respectable metals, such as Zr and Ce, essentially expanded the activity and lifetime of the catalyst [64]. According to the above, the high selectivity for C_{5+} was about 91.66% when the prepared cobalt catalysts promoted with Ce were used in the present study.

5. Conclusions

In the current investigation, catalytic tests for Fischer–Tropsch synthesis were carried out in a fixed-bed reactor over a Ce-Co/SiO_2 catalyst. The impregnation process was used to create the catalyst. At various operating temperatures, pressures, gas hourly space velocities (GHSV), and syngas ratios (H_2/CO), sixteen experiments were conducted. The proposed kinetic model was logically investigated using statistical and correlation tests. As a result, the results show that the estimated activation energies' values were consistent with those provided by earlier investigations. The Matlab 2020a programming language was used to code all of the computations in this investigation. An isothermal plug flow reactor model was used to simulate the lab reactor, and a MATLAB ordinary differential equation solver was used to resolve a set of species mass balance equations. A genetic algorithm was utilized to estimate the ideal set of kinetic parameters. The statistical test found the estimated parameters and thorough kinetic model to be statistically significant. The established model predicts a fraction of the reactants and products over the length of the reactor bed.

Author Contributions: Validation, I.H. Writing—original draft, F.K.A.-Z.; Writing—review & editing, F.K.A.-Z., Z.M.S. and I.H. All authors have read and agreed to the published version of the manuscript.

Funding: This research received no external funding.

Data Availability Statement: All data used in the present study appear in the submitted article.

Conflicts of Interest: The authors declare no conflict of interest.

Nomenclature

Ci	Concentration of component i	$mol.cm^{-3}$
Ea	Activation energy	kJ/mol
F_i	Molar flow rate of component i	mole/s
k_j	Rate constant of reaction j	mol/gcat·h·bar
k_j^0	Pre-exponential factor	mol/gcat·h·bar
M_m	Average molecular weight	kg/mole
nj, mj	Orders of reaction rate j	-
P_t	Total pressure	bar
P_i	Partial pressure of component i	bar
R	Universal gas constant	8.3145 J/mole. K
r_j	Rate of reaction j	mole/gm cat·h
Si	Selectivity for component i mole	%
$s_{i,j}$	Stoichiometric coefficient for the ith component participating in the jth reaction	
T	Temperature	K
w	Amount of catalyst in the reactor	Gm
xi	mole fraction of component i in the liquid phase	-
yi	mole fraction of component i in the gas phase	-

Abbreviations

FTS	Fischer–Tropsch Synthesis
GA	Genetic Algorithm
LHHW	Langmuir–Hinshelwood–Hougen–Watts
MARE	Mean absolute relative error
cat	Catalyst
com	Component
exp	Experimental value
H	Hydrogen

References

1. Pandey, U.; Runningen, A.; Gavrilović, L.; Jørgensen, E.A.; Putta, K.R.; Rout, K.R.; Rytter, E.; Blekkan, E.A.; Hillestad, M. Modeling Fischer–Tropsch kinetics and product distribution over a cobalt catalyst. *AIChE J.* **2021**, *67*, e17234. [CrossRef]
2. Al-Zuhairi, F.K.; Azeez, R.A.; Mahdi, S.A. Synthesis of long-chain hydrocarbons from Syngas over promoted Co/SiO_2 catalysts using Fischer–Tropsch reaction. *AIP Conf. Proc.* **2022**, *2443*, 030028.
3. Steynberg, A. Introduction to fischer-tropsch technology. In *Studies in Surface Science and Catalysis*; Elsevier: Amsterdam, The Netherlands, 2004; Volume 152, pp. 1–63.
4. Van Santen, R.; Markvoort, A.; Filot, I.; Ghouri, M.; Hensen, E. Mechanism and microkinetics of the Fischer–Tropsch reaction. *Phys. Chem. Chem. Phys.* **2013**, *15*, 17038–17063. [CrossRef] [PubMed]
5. Al-Zuhairi, F.; Micoli, L.; Florio, C.; Ausiello, A.; Turco, M.; Pirozzi, D.; Toscano, G. Anaerobic co-digestion of municipal solid wastes with giant reed under mesophilic conditions. *J. Mater. Cycles Waste Manag.* **2019**, *21*, 1332–1340. [CrossRef]
6. Sukkar, K.A.; Al-Zuhairi, F.K.; Dawood, E.A. Evaluating the Influence of Temperature and Flow Rate on Biogas Production from Wood Waste via a Packed-Bed Bioreactor. *Arab. J. Sci. Eng.* **2021**, *46*, 6167–6175. [CrossRef]
7. León, E.; Martín, M. Optimal production of power in a combined cycle from manure based biogas. *Energy Convers. Manag.* **2016**, *114*, 89–99. [CrossRef]
8. Hernandez, B.; Martin, M. Optimization for biogas to chemicals via tri-reforming. Analysis of Fischer-Tropsch fuels from biogas. *Energy Convers. Manag.* **2018**, *174*, 998–1013. [CrossRef]
9. Xie, J.; Paalanen, P.P.; van Deelen, T.W.; Weckhuysen, B.M.; Louwerse, M.J.; de Jong, K.P. Promoted cobalt metal catalysts suitable for the production of lower olefins from natural gas. *Nat. Commun.* **2019**, *10*, 167. [CrossRef]
10. Zhang, Q.; Cheng, K.; Kang, J.; Deng, W.; Wang, Y. Fischer–Tropsch catalysts for the production of hydrocarbon fuels with high selectivity. *ChemSusChem* **2014**, *7*, 1251–1264. [CrossRef]
11. Moazami, N.; Mahmoudi, H.; Panahifar, P.; Rahbar, K.; Tsolakis, A.; Wyszynski, M.L. Mathematical modeling and performance study of Fischer-Tropsch synthesis of liquid fuel over cobalt-silica. *Energy Procedia* **2015**, *75*, 62–71. [CrossRef]
12. Zhu, C.; Bollas, G.M. Gasoline selective Fischer-Tropsch synthesis in structured bifunctional catalysts. *Appl. Catal. B Environ.* **2018**, *235*, 92–102. [CrossRef]
13. Pardo-Tarifa, F.; Cabrera, S.; Sanchez-Dominguez, M.; Boutonnet, M. Ce-promoted Co/Al_2O_3 catalysts for Fischer–Tropsch synthesis. *Int. J. Hydrog. Energy* **2017**, *42*, 9754–9765. [CrossRef]
14. Moazami, N.; Wyszynski, M.L.; Rahbar, K.; Tsolakis, A.; Mahmoudi, H. A comprehensive study of kinetics mechanism of Fischer-Tropsch synthesis over cobalt-based catalyst. *Chem. Eng. Sci.* **2017**, *171*, 32–60. [CrossRef]
15. Egiebor, N.; Ungar, K.; Wojciechowski, B. A classification of fischer–tropsch synthesis product distributions. *Can. J. Chem. Eng.* **1984**, *62*, 425–430. [CrossRef]
16. Irani, M. Modeling of Fischer-Tropsch Synthesis Packed Bed Reactor for Producing Liquid Fuels from Natural Gas. *Pet. Coal* **2013**, *55*, 82–92.
17. Moazami, N.; Mahmoudi, H.; Rahbar, K.; Panahifar, P.; Tsolakis, A.; Wyszynski, M.L. Catalytic performance of cobalt–silica catalyst for Fischer–Tropsch synthesis: Effects of reaction rates on efficiency of liquid synthesis. *Chem. Eng. Sci.* **2015**, *134*, 374–384. [CrossRef]
18. Mosayebi, A.; Haghtalab, A. The comprehensive kinetic modeling of the Fischer–Tropsch synthesis over Co@ Ru/γ-Al_2O_3 core–shell structure catalyst. *Chem. Eng. J.* **2015**, *259*, 191–204. [CrossRef]
19. Atashi, H.; Gholizadeh, J.; Tabrizi, F.F.; Tayebi, J. Modeling selectivity of ethylene and propylene in the Fischer-Tropsch synthesis with artificial neural network and response surface methodology. *ChemistrySelect* **2016**, *1*, 3271–3275. [CrossRef]
20. Hatami, B.; Tavasoli, A.; Asghari, A.; Zamani, Y.; Zamaniyan, A. Kinetics Modeling of Fischer–Tropsch Synthesis on the Cobalt Catalyst Supported on Functionalized Carbon Nanotubes. *Kinet. Catal.* **2018**, *59*, 701–709. [CrossRef]
21. Haghtalab, A.; Shariati, J.; Mosayebi, A. Experimental and kinetic modeling of Fischer–Tropsch synthesis over nano structure catalyst of Co–Ru/carbon nanotube. *React. Kinet. Mech. Catal.* **2019**, *126*, 1003–1026. [CrossRef]
22. Zohdi-Fasaei, H.; Atashi, H.; Farshchi Tabrizi, F.; Mirzaei, A.A. Modeling and optimization of Fischer-Tropsch synthesis over $Co-Mn-Ce/SiO_2$ catalyst using hybrid RSM/LHHW approaches. *Energy* **2017**, *128*, 496–508. [CrossRef]
23. Barkalov, K.; Gubaydullin, I.; Kozinov, E.; Lebedev, I.; Faskhutdinova, R.; Faskhutdinov, A.; Enikeeva, L. On Solving the Problem of Finding Kinetic Parameters of Catalytic Isomerization of the Pentane-Hexane Fraction Using a Parallel Global Search Algorithm. *Mathematics* **2022**, *10*, 3665. [CrossRef]
24. Nestler, F.; Müller, V.; Ouda, M.; Hadrich, M.; Schaadt, A.; Bajohr, S.; Kolb, T. A novel approach for kinetic measurements in exothermic fixed bed reactors: Advancements in non-isothermal bed conditions demonstrated for methanol synthesis. *React. Chem. Eng.* **2021**, *6*, 1092–1107. [CrossRef]
25. Parsafard, N.; Garmroodi, A.; Mirzaei, S. Gas-phase catalytic isomerization of n-heptane using $Pt/(CrOx/ZrO_2)$-HMS catalysts: A kinetic modeling. *Int. J. Chem. Kinet.* **2021**, *53*, 971–981. [CrossRef]
26. Shakor, Z.M.; AbdulRazak, A.A.; Sukkar, K.A. A detailed reaction kinetic model of heavy naphtha reforming. *Arab. J. Sci. Eng.* **2020**, *45*, 7361–7370. [CrossRef]
27. Shakor, Z.M.; Ramos, M.J.; AbdulRazak, A.A. A detailed reaction kinetic model of light naphtha isomerization on Pt/zeolite catalyst. *J. King Saud. Univ. Eng. Sci.* **2022**, *34*, 303–308. [CrossRef]

28. Regali, F.; Boutonnet, M.; Järås, S. Hydrocracking of n-hexadecane on noble metal/silica–alumina catalysts. *Catal. Today* **2013**, *214*, 12–18. [CrossRef]
29. Ancheyta-Juárez, J.; Villafuerte-Macías, E. Kinetic modeling of naphtha catalytic reforming reactions. *Energy Fuels* **2000**, *14*, 1032–1037. [CrossRef]
30. Al-Shathr, A.; Shakor, Z.M.; Majdi, H.S.; AbdulRazak, A.A.; Albayati, T.M. Comparison between artificial neural network and rigorous mathematical model in simulation of industrial heavy naphtha reforming process. *Catalysts* **2021**, *11*, 1034. [CrossRef]
31. Aammer, H.; Shakor, Z.M.; Al-Sheikh, F.; Al-Naimi, S.A.; Anderson, W.A. Simulation and Optimization of the Ethane Cracking Furnace Using ASPEN PLUS and MATLAB: A Case Study from Petrochemical Complexes. *Combust. Sci. Technol.* **2022**, *195*, 2634–2654. [CrossRef]
32. Hájek, J.; Murzin, D.Y. Liquid-Phase Hydrogenation of Cinnamaldehyde over a Ru−Sn Sol−Gel Catalyst. 1. Evaluation of Mass Transfer via a Combined Experimental/Theoretical Approach. *Ind. Eng. Chem. Res.* **2004**, *43*, 2030–2038. [CrossRef]
33. Khalaf, Y.H.; Al-Zaidi, B.Y.S.; Shakour, Z.M. Experimental and Kinetic Study of the Effect of using Zr-and Pt-loaded Metals on Y-zeolite-based Catalyst to Improve the Products of n-heptane Hydroisomerization Reactions. *Orbital Electron. J. Chem.* **2022**, *14*, 153–167. [CrossRef]
34. Al-Shathr, A.; Shakor, Z.M.; Al-Zaidi, B.Y.; Majdi, H.S.; AbdulRazak, A.A.; Aal-Kaeb, S.; Shohib, A.A.; McGregor, J. Reaction Kinetics of Cinnamaldehyde Hydrogenation over Pt/SiO_2: Comparison between Bulk and Intraparticle Diffusion Models. *Int. J. Chem. Eng.* **2022**, *2022*, 8303874. [CrossRef]
35. Al-Karim, A.A.; Shakor, Z.M.; Al-Sheikh, F.; Anderson, W.A. Experimental and kinetic study of vacuum residue cracking over zirconium based catalysts. *React. Kinet. Mech. Catal.* **2022**, *135*, 847–865. [CrossRef]
36. Khalaf, A.L.; Al-Zuhairi, F.K.; Kadhim, W.A.; Ab Rahim, M.H. The effects of cerium promoter on the performance of cobalt-based catalysts in fischer tropsch synthesis for liquid fuel production. *IIUM Eng. J.* **2020**, *21*, 1–11. [CrossRef]
37. Gnanamani, M.K.; Jacobs, G.; Graham, U.M.; Pendyala, V.R.R.; Martinelli, M.; MacLennan, A.; Hu, Y.; Davis, B.H. Effect of sequence of P and Co addition over silica for Fischer-Tropsch synthesis. *Appl. Catal. A Gen.* **2017**, *538*, 190–198. [CrossRef]
38. Xue, L.; Zhang, C.; He, H.; Teraoka, Y. Catalytic decomposition of N_2O over CeO_2 promoted Co_3O_4 spinel catalyst. *Appl. Catal. B Environ.* **2007**, *75*, 167–174. [CrossRef]
39. Xiaoping, D.; Changchun, Y.; Ranjia, L.; Haibo, S.; Shikong, S. Role of CeO_2 promoter in Co/SiO_2 catalyst for Fischer-Tropsch synthesis. *Chin. J. Catal.* **2006**, *27*, 904–910.
40. Eliseev, O.; Tsapkina, M.; Davydov, P.; Dzhukasheva, L.; Lapidus, A. Synthesis of hydrocarbons from carbon monoxide and hydrogen in the presence of cobalt catalysts promoted with cerium oxide. *Solid Fuel Chem.* **2017**, *51*, 166–169. [CrossRef]
41. Mansouri, M.; Atashi, H.; Mirzaei, A.A.; Jangi, R. Kinetics of the Fischer-Tropsch synthesis on silica-supported cobalt-cerium catalyst. *Int. J. Ind. Chem.* **2013**, *4*, 1. [CrossRef]
42. Mansouri, M.; Atashi, H.; Tabrizi, F.F.; Mansouri, G.; Setareshenas, N. Fischer–Tropsch synthesis on cobalt–manganese nanocatalyst: Studies on rate equations and operation conditions. *Int. J. Ind. Chem.* **2014**, *5*, 14. [CrossRef]
43. Dry, M.E. Practical and theoretical aspects of the catalytic Fischer-Tropsch process. *Appl. Catal. A Gen.* **1996**, *138*, 319–344. [CrossRef]
44. Zolfaghari, Z.; Tavasoli, A.; Tabyar, S.; Pour, A.N. Enhancement of bimetallic Fe-Mn/CNTs nano catalyst activity and product selectivity using microemulsion technique. *J. Energy Chem.* **2014**, *23*, 57–65. [CrossRef]
45. Pendyala, V.R.R.; Jacobs, G.; Bertaux, C.; Khalid, S.; Davis, B.H. Fischer–Tropsch synthesis: Effect of ammonia on supported cobalt catalysts. *J. Catal.* **2016**, *337*, 80–90. [CrossRef]
46. Zhang, L.; Chu, H.; Qu, H.; Zhang, Q.; Xu, H.; Cao, J.; Tang, Z.; Xuan, J. An investigation of efficient microstructured reactor with monolith Co/anodic γ-Al_2O_3/Al catalyst in Fischer-Tropsch synthesis. *Int. J. Hydrog. Energy* **2018**, *43*, 3077–3086. [CrossRef]
47. Akbarzadeh, O.; Mohd Zabidi, N.A.; Wang, G.; Kordijazi, A.; Sadabadi, H.; Moosavi, S.; Amani Babadi, A.; Hamizi, N.A.; Abdul Wahab, Y.; Ab Rahman, M. Effect of Pressure, H_2/CO Ratio and Reduction Conditions on Co–Mn/CNT Bimetallic Catalyst Performance in Fischer–Tropsch Reaction. *Symmetry* **2020**, *12*, 698. [CrossRef]
48. Tristantini, D.; Lögdberg, S.; Gevert, B.; Borg, Ø.; Holmen, A. The effect of synthesis gas composition on the Fischer–Tropsch synthesis over Co/γ-Al_2O_3 and $Co–Re/\gamma$-Al_2O_3 catalysts. *Fuel Process. Technol.* **2007**, *88*, 643–649. [CrossRef]
49. Pant, K.K.; Upadhyayula, S. Detailed kinetics of Fischer Tropsch synthesis over Fe-Co bimetallic catalyst considering chain length dependent olefin desorption. *Fuel* **2019**, *236*, 1263–1272.
50. Ghouri, M.M.; Afzal, S.; Hussain, R.; Blank, J.; Bukur, D.B.; Elbashir, N.O. Multi-scale modeling of fixed-bed Fischer Tropsch reactor. *Comput. Chem. Eng.* **2016**, *91*, 38–48. [CrossRef]
51. Okeke, I.J.; Sahoo, K.; Kaliyan, N.; Mani, S. Life cycle assessment of renewable diesel production via anaerobic digestion and Fischer-Tropsch synthesis from miscanthus grown in strip-mined soils. *J. Clean. Prod.* **2020**, *249*, 119358. [CrossRef]
52. Okeke, I.J.; Mani, S. Techno-economic assessment of biogas to liquid fuels conversion technology via Fischer-Tropsch synthesis. *Biofuels Bioprod. Biorefining* **2017**, *11*, 472–487. [CrossRef]
53. Naqi, A.; Kuhn, J.N.; Joseph, B. Techno-economic analysis of producing liquid fuels from biomass via anaerobic digestion and thermochemical conversion. *Biomass Bioenergy* **2019**, *130*, 105395. [CrossRef]
54. Tijmensen, M.J.; Faaij, A.P.; Hamelinck, C.N.; van Hardeveld, M.R. Exploration of the possibilities for production of Fischer Tropsch liquids and power via biomass gasification. *Biomass Bioenergy* **2002**, *23*, 129–152. [CrossRef]

55. Swanson, R.M.; Platon, A.; Satrio, J.A.; Brown, R.C. Techno-economic analysis of biomass-to-liquids production based on gasification. *Fuel* **2010**, *89*, S11–S19. [CrossRef]
56. Hamelinck, C.N.; Faaij, A.P.; den Uil, H.; Boerrigter, H. Production of FT transportation fuels from biomass; technical options, process analysis and optimisation, and development potential. *Energy* **2004**, *29*, 1743–1771. [CrossRef]
57. Kauffman, N.; Hayes, D.; Brown, R. A life cycle assessment of advanced biofuel production from a hectare of corn. *Fuel* **2011**, *90*, 3306–3314. [CrossRef]
58. De Jong, S.; Antonissen, K.; Hoefnagels, R.; Lonza, L.; Wang, M.; Faaij, A.; Junginger, M. Life-cycle analysis of greenhouse gas emissions from renewable jet fuel production. *Biotechnol. Biofuels* **2017**, *10*, 64. [CrossRef] [PubMed]
59. Dang, Q.; Yu, C.; Luo, Z. Environmental life cycle assessment of bio-fuel production via fast pyrolysis of corn stover and hydroprocessing. *Fuel* **2014**, *131*, 36–42. [CrossRef]
60. Fortier, M.-O.P.; Roberts, G.W.; Stagg-Williams, S.M.; Sturm, B.S. Life cycle assessment of bio-jet fuel from hydrothermal liquefaction of microalgae. *Appl. Energy* **2014**, *122*, 73–82. [CrossRef]
61. Dry, M.E. Fischer-Tropsch synthesis over iron catalysts. *Catal. Lett.* **1990**, *7*, 241–251. [CrossRef]
62. Rytter, E.; Tsakoumis, N.E.; Holmen, A. On the selectivity to higher hydrocarbons in Co-based Fischer–Tropsch synthesis. *Catal. Today* **2016**, *261*, 3–16. [CrossRef]
63. Khodakov, A.Y. Fischer-Tropsch synthesis: Relations between structure of cobalt catalysts and their catalytic performance. *Catal. Today* **2009**, *144*, 251–257. [CrossRef]
64. Borg, Ø.; Eri, S.; Blekkan, E.A.; Storsæter, S.; Wigum, H.; Rytter, E.; Holmen, A. Fischer–Tropsch synthesis over γ-alumina-supported cobalt catalysts: Effect of support variables. *J. Catal.* **2007**, *248*, 89–100. [CrossRef]